http://dx.doi.org/10.5012/bkcs.2013.34.4.1205

Effects of Doping with Al, Ga, and In on Structural and Optical Properties of ZnO Nanorods Grown by Hydrothermal Method

Soaram Kim, Giwoong Nam, Hyunggil Park, Hyunsik Yoon, Sang-heon Lee,[†] Jong Su Kim,[‡] Jin Soo Kim,[§] Do Yeob Kim,[#] Sung-O Kim,[#] and Jae-Young Leem[*]

Department of Nano Systems Engineering, Center for Nano Manufacturing, Inje University, Gimhae, Gyungnam 621-749, Korea
[*]E-mail: jyleem@inje.ac.kr
[†]School of Chemical Engineering, Yeungnam University, Gyeongsan, Gyeongbuk 712-749, Korea
[‡]Department of Physics, Yeungnam University, Gyeongsan, Gyeongbuk 712-749, Korea
[§]Research Center of Advanced Materials Development (RCAMD), Division of Advanced Materials Engineering, Chonbuk National University, Jeonju, Chonbuk 561-756, Korea
[#]Holcombe Department of Electrical and Computer Engineering, Center for Optical Materials Science and Engineering Technologies (COMSET), Clemson University, Clemson, SC 29634, USA
Received November 22, 2012, Accepted January 30, 2013

The structural and optical properties of the ZnO, Al-doped ZnO, Ga-doped ZnO, and In-doped ZnO nanorods were investigated using field-emission scanning electron microscopy, X-ray diffraction, photoluminescence (PL) and ultraviolet-visible spectroscopy. All the nanorods grew with good alignment on the ZnO seed layers and the ZnO nanorod dimensions could be controlled by the addition of the various dopants. For instance, the diameter of the nanorods decreased with increasing atomic number of the dopants. The ratio between the near-band-edge emission (NBE) and the deep-level emission (DLE) intensities (I_{NBE}/I_{DLE}) obtained by PL gradually decreased because the DLE intensity from the nanorods gradually increased with increase in the atomic number of the dopants. We found that the dopants affected the structural and optical properties of the ZnO nanorods including their dimensions, lattice constants, residual stresses, bond lengths, PL properties, transmittance values, optical band gaps, and Urbach energies.

Key Words : Zinc oxide, Doping, Hydrothermal, Photoluminescence, Transmittance

Introduction

Zinc oxide (ZnO) is a widely used functional material that exhibits a wide direct band gap (3.37 eV at 300 K), high exciton binding energy (60 meV), and excellent chemical and thermal stabilities.[1] Therefore, ZnO is an excellent candidate for application in light emitting diodes,[2] laser diodes,[3] field emission devices,[4] chemical sensors,[5] and solar cells.[6] In recent years, applications of ZnO nanostructures, particularly nanorods, in dye sensitized solar cells and thermoelectronics have attracted increasing interest.[7-9] In order to improve the optical and electrical properties of ZnO nanorods, group III elements such as Al,[10,11] Ga,[12,13] and In[14,15] can be used as cation dopants. Al-doped ZnO (AZO), Ga-doped ZnO (GZO), and In-doped ZnO (IZO) nanorods can be used as transparent electrodes in optoelectronic devices. Consequently, considerable efforts have been devoted toward improving the optical and electrical properties of ZnO nanorods by doping. Hence, it is important to understand the influence of the dopants on the structural, optical, and electrical properties of ZnO nanorods prior to employing these materials in practical applications.

ZnO nanorods can be grown using various methods such as chemical vapor deposition (CVD),[16] vapor phase transport (VPT),[17] and hydrothermal methods.[18] Among these, hydrothermal methods enables the preparation of ZnO nanorods at much lower temperatures, which makes the process more effective, simplifies the control of dopant concentrations, and allows the use of simple equipment.[19] The preparation of ZnO nanorods by hydrothermal method requires three steps. In the first step, which is perhaps the most important among the three, the ZnO seed layers are deposited. Then, randomly oriented ZnO crystals are grown from the seed layers. Finally, due to the collisions between the randomly oriented ZnO crystals, extended ZnO nanorods are grown to form arrays. In these arrays, the *c*-axis of the nanorods is perpendicular to the substrate surface.[20]

Although there are systematically many publications reporting on various dopants in ZnO thin films,[21-23] there is a lack of research on various dopants for ZnO nanorods. In addition, most research is reporting on a dopant in ZnO nanorods or nanostructures[10,24,14] and GZO and IZO nanorods are rare in hydrothermal method. Hence, with the aim to further understand the structural and optical properties of ZnO nanorods by various dopants, we herein investigated the effect of Al, Ga, and In doping on ZnO nanorods in this study.

Experimental Details

The ZnO seed layers were deposited on the quartz substrates using the sol-gel spin coating method. The sol solu-

tion was prepared by dissolving 0.6 M zinc acetate dihydrate [$Zn(CH_3OO)_2{\cdot}2H_2O$] in 0.6 M 2-methoxyethanol as a solvent with monoethanolamine (MEA) added to the stable sol solution. The molar ratio of zinc acetate to MEA was 1:1 for all experiments carried out in this study. The resultant sol solutions were stirred at 60 °C for 2 h to yield a clear and homogeneous solution before being aged at room temperature for 24 h. The sol solution was spin-coated onto the quartz substrate and rotated at 3,000 rpm for 20 s. After deposition by spin-coating, the ZnO seed layers were pre-heated at 300 °C for 10 min to evaporate the solvent and to remove the residual organic materials. After this pre-heating, the ZnO seed layers were cooled at a rate of 5 °C/min to prevent the formation of cracks. The coating and pre-heating procedures were repeated three times, and the ZnO seed layers were then post-heated in a furnace at 550 °C in air for 1 h.

As mentioned earlier, ZnO, AZO, GZO, and IZO nanorods were grown on the ZnO seed layers by hydrothermal methods. The ZnO seed layers were rinsed with deionized (DI) water and immersed in a mixture of aqueous 0.1 M zinc nitrate hexahydrate [$Zn(NO_3)_2{\cdot}6H_2O$], 0.1 M hexamethylenetetramine (HMT) [$(CH_2)_6N_4$], and an aqueous solution of a salt containing the dopant cation. The mixture was confined in a Teflon-lined autoclave. In our study, aqueous solutions of aluminum(III) nitrate nonahydrate [$Al(NO_3)_3{\cdot}9H_2O$], gallium(III) nitrate hydrate [$Ga(NO_3)_3{\cdot}xH_2O$], and indium(III) chloride [$InCl_3$] were used as the Al, Ga, and In dopant precursors, respectively. In the mixture, the Al/Zn, Ga/Zn, In/Zn ratios were fixed at 2.0 at %. The nanorods growth was carried out by maintaining the temperature of the autoclave at 95 °C for 4 h. After the completion of the reaction, the substrate was rinsed with DI water and blow dried with ultra-high-purity (99.9999%) nitrogen to remove residual salts and organic materials. The structural and optical properties of the ZnO, AZO, GZO, and IZO nanorods obtained were then investigated using scanning electron microscopy (SEM), X-ray diffraction (XRD), photoluminescence (PL), and ultraviolet-visible spectroscopy.

Results and Discussion

Figure 1 shows the SEM images of (a) ZnO, (b) AZO, (c) GZO, (d) IZO nanorods, and (e) ZnO seed layers. First, the thickness of the seed layers is 72 nm and a dense and uniform surface are observed in ZnO seed layers prepared by the conventional sol-gel method as shown in Figure 1(e). As already stated vide supra, ZnO seed layers are required for the growth of ZnO nanorods. In our previous study,[18,19,25-28] we studied the effect of seed layers on the growth of ZnO nanorods. All the nanorods were hexagonal in shape and were well-grown on the ZnO seed layers. The typical lengths and diameters of the ZnO, AZO, GZO, and IZO nanorods were 1064 and 90 nm, 440 and 180 nm, 160 and 116 nm, 820 and 70 nm, respectively. It is worth noting that we could control the size of the nanorods by adding different dopants during the nanorods growth because doping of the ZnO

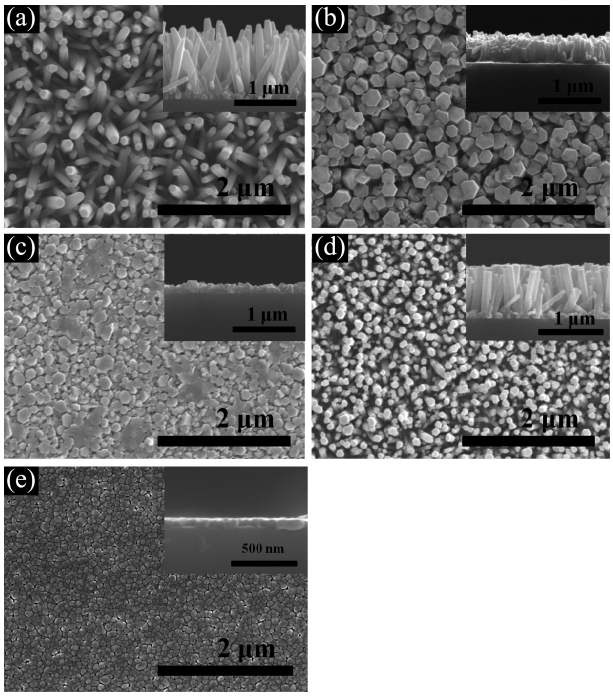

Figure 1. SEM images of (a) ZnO, (b) AZO, (c) GZO, (d) IZO nanorods, and (e) ZnO seed layers.

lattice was achieved by interstitial and/or substitution reaction. It can be seen that the diameter of the nanorods specifically decreased with increasing dopant atomic number. The atomic radius, which is related to the atomic number, increases with increase in the atomic number for group III elements (dopants). The atomic radii of Zn, Al, Ga, and In are 1.35, 1.25, 1.30, 1.55 Å, respectively. The differences in the atomic radii between Zn and the dopants could probably have resulted in the decrease of the nanorods diameters. The mechanism for the growing of the ZnO, AZO, GZO, and IZO nanorods using HMT can be summarized in the following equations:

$$(CH_2)_6N_4 + 6H_2O \rightarrow 6COH_2 + 4NH_3 \quad (1)$$

$$NH_3 + H_2O \rightarrow NH_4^+ + OH^- \quad (2)$$

$$Zn(NO_3)_2{\cdot}6H_2O \rightarrow Zn^{2+} + 2NO_3^- + 6H_2O \quad (3)$$

$$Zn^{2+} + 2OH^- \rightarrow Zn(OH)_2 \rightarrow ZnO + H_2O \quad (4)$$

$$Al(NO_3)_3{\cdot}9H_2O \rightarrow Al^{3+} + 3NO_3^- + 9H_2O \quad (5)$$

$$4Al^{3+} + 12OH^- \rightarrow 2Al_2O_3 + 6H_2O \quad (6)$$

$$Ga(NO_3)_3{\cdot}xH_2O \rightarrow Ga^{3+} + 3NO_3^- + xH_2O \quad (7)$$

$$4Ga^{3+} + 12OH^- \rightarrow 2Ga_2O_3 + 6H_2O \quad (8)$$

$$InCl_3 \rightarrow In^{3+} + 3Cl^- \quad (9)$$

$$4In^{3+} + 12OH^- \rightarrow 2In_2O_3 + 6H_2O \quad (10)$$

Zn^{2+} are known to react readily with OH^- to form more soluble $Zn(OH)_2$ complexes, which act as the growth unit of ZnO nanorods. Finally ZnO nanorods is obtained by decomposition of $Zn(OH)_2$. Therefore, the key parameter for the growth of ZnO nanorods is controlling the supersaturation of the reactants as Eq. (4).[18] Also, HMT plays a very complicated role in the solution during the hydro-

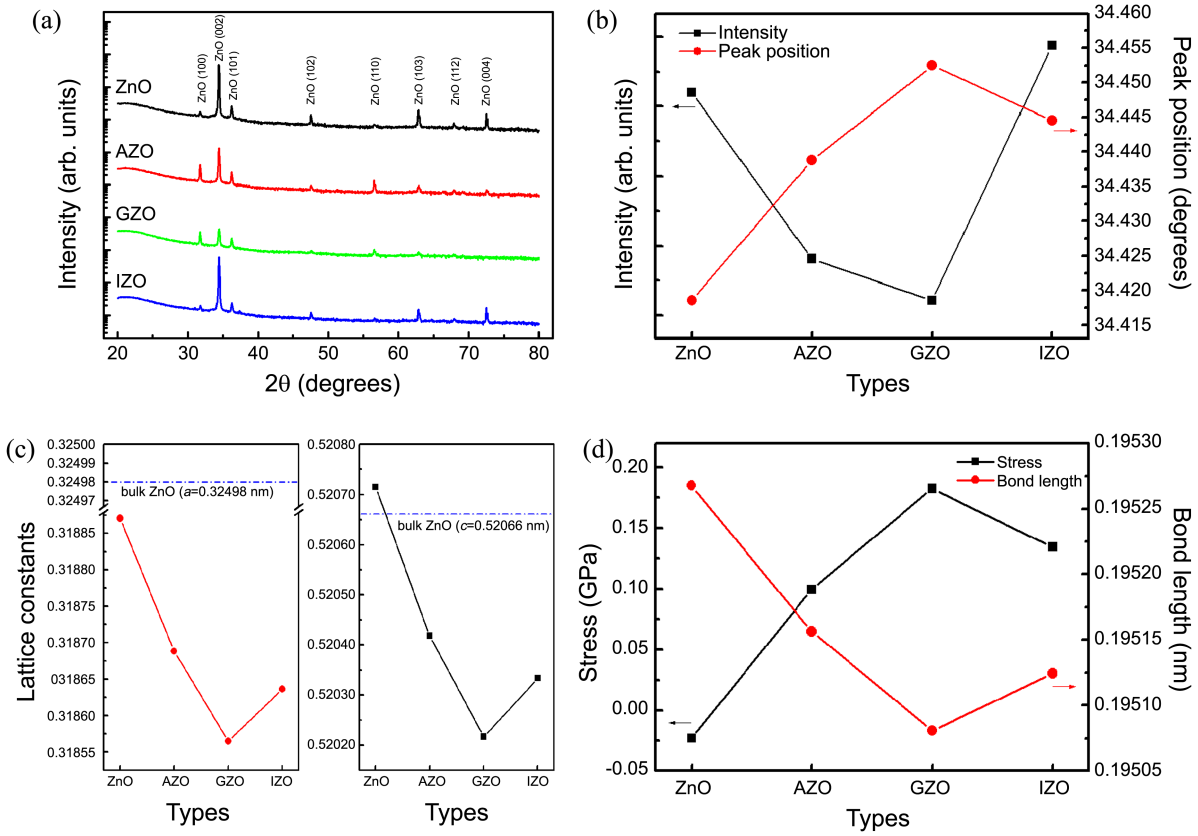

Figure 2. (a) XRD patterns, (b) (002) intensity and peak position, (c) lattice constants, and (d) residual stress and bond length values shown by ZnO, AZO, GZO, and IZO nanorods.

thermal method,[29] and it supplies OH^- to the Zn^{2+}, Al^{3+}, Ga^{3+}, and In^{3+} to form Zn-O, Al-O, Ga-O, and In-O bonds here, respectively. Thereby, doping of the ZnO lattice was achieved by interstitial and/or substitution reaction.

Figure 2(a) shows the XRD patterns acquired from the ZnO, AZO, GZO, and IZO nanorods samples, respectively. The patterns from all the nanorod samples was dominated by the (002) peak of wurtzite-type ZnO, implying that the preferred orientation of the ZnO nanorods was along the (002) direction. This could be ascribed to the rapid vertical growth rate of the nanorods and their limited growth along the lateral difrection.[30] The intensities of the (002) peak were proportional to the lengths and densities of the nanorods. In the case of GZO nanorods sample, the (002) peak intensity was the lowest among all the specimens. This was because the length of the GZO nanorods was the smallest when compared to all other samples. However, the IZO nanorods sample, containing the longest and most densely packed nanorods, exhibited the most intense (002) peak among all the samples, as shown in Figure 2(b). As can be observed from Figure 1 and Figure 2(a), Ga doping resulted in low nanorods growth rate and decreased wurtzite (002) peak intensities in the XRD patterns. The effect was prominently observed in GZO nanorods, suggesting a loss in the crystallinity of the nanorods because of the substitution reaction between Zn and Ga. We attribute the occurrence of the substitution reaction to the similarity in the atomic radii of Zn and Ga. However, we propose that the higher difference in the atomic radii between Zn and the doping atoms Al and In probably led to interstitial reactions, which may have resulted in higher growth rates and increasingly intense ZnO (002) peaks in the XRD patterns, when compared to doping with Ga. In addition, the various dopants also shifted the (002) peak position of ZnO toward higher 2θ values, as shown in Figure 2(b). Among the various samples, peak position of the GZO nanorods showed the maximum-shift to higher 2θ values. This could be attributed to the decrease of interplanar spacing in the crystals due to the substitution of Zn by Ga. In addition, the effect of doping could also be observed in the lattice constants, as shown in Figure 2(c). In general, the lattice constants of the as-grown ZnO are close to the values reported for ZnO (a = 0.32498 nm and c = 0.52066 nm) by Heller *et al.*[31] From our experiments, the lattice constants of ZnO, AZO, GZO, and IZO were found to be a = 0.31887 and c = 0.52071 nm, a = 0.31868 and c = 0.52041 nm, a = 0.31856 and c = 0.52021 nm, and a = 0.31863 and c = 0.52033 nm. The differences in the lattice constants was distinct, which suggested that the incorporated dopants may have occupied specific lattice sites, resulting in the anisotropic distortion of the unit cell along the (001) direction. Hence, incorporation of the dopants caused considerable distortion of the ZnO lattice and affected the lattice structure and/or crystallinity of the ZnO nanorods. In the case of AZO nanorods, the lattice constants were close to the

reported values, while the GZO nanorods exhibited the maximum shift in the lattice constants among the doped nanorods samples. The calculated lattice constant values for ZnO can be expressed as follows:[32]

$$c = 2d_{002} = \lambda/\sin\theta \quad (11)$$

where λ is the wavelength of the Cu-Kα radiation (1.5406 Å) and θ is the Bragg angle. Figure 2(d) shows the residual stress, σ, and bond length, L, of the ZnO, AZO, GZO, and IZO nanorods. A residual stress is generated in the ZnO nanorods because of the differences in the lattice constants and the thermal expansion coefficients between the ZnO and the substrate. The residual stress in the ZnO nanorods can be calculated as follows:[33]

$$\sigma = [2C_{13}^2 - C_{33}(C_{11} + C_{12})/2C_{13}] \times [(c - c_0)/c_0], \quad (12)$$

where C_{ij} are the elastic stiffness constants for ZnO (C_{11} = 207.0, C_{33} = 209.5, C_{12} = 117.7, and C_{13} = 106.1 GPa), and c and c_0 are the lattice parameters of the ZnO and strain-free ZnO, respectively. If the stress is positive, the biaxial stress will be tensile; if the stress is negative, the biaxial stress will be compressive. The stresses values in the ZnO, AZO, GZO, and IZO nanorods were calculated as −0.022, 0.099, 0.182, and 0.134 GPa. Hence, the nature of stress altered from compressive to tensile with doping and among the doped nanorods, the stress in AZO nanorods was closest to that shown by strain-free ZnO. The Zn-O bond length in the ZnO nanorods is given by[34]

$$L = \sqrt{(a^2/3) + \{(1/2) - u\}^2 \times c^2}, \quad (13)$$

where (in the wurtzite structure) u is given by

$$u = (a^2/3c^2) + 0.25 \quad (14)$$

and u is related to the a/c ratio. The values of L were found to be 0.19526, 0.19515, 0.19508, and 0.19512 nm in the ZnO, AZO, GZO, and IZO nanorods, respectively, as shown in Figure 2(d).

Figure 3(a) shows the normalized PL spectra acquired from the ZnO, AZO, GZO, and IZO nanorods. All the normalized PL spectra exhibited the near-band-edge emission (NBE), generated by free-exciton recombination[35] at 3.261, 3.279, 3.244, and 3.272 eV for ZnO, AZO, GZO, and IZO nanorods, respectively. In addition, broad deep-level emission (DLE) was also observed at about 2.238 (green emission), 2.188 (green emission), 2.082 (orange emission), and 2.184 eV (green emission) for ZnO, AZO, GZO, and IZO nanorods, respectively. The DLE is usually attributed to the presence of structural defects. Interestingly, the NBE and DLE peaks were shifted by the various dopants. In the case of NBE, when compared to the peak from the ZnO nanorods (3.261 eV), the peak originating from GZO nanorods was shifted to a lower energy value (3.244 eV). However, the NBE peaks from AZO and IZO nanorods were shifted to higher energies to 3.279 and 3.272 eV, respectively. In the case of DLE, the intensities of the peaks were increased by the presence of the dopants, which may have acted as impurities in the pure

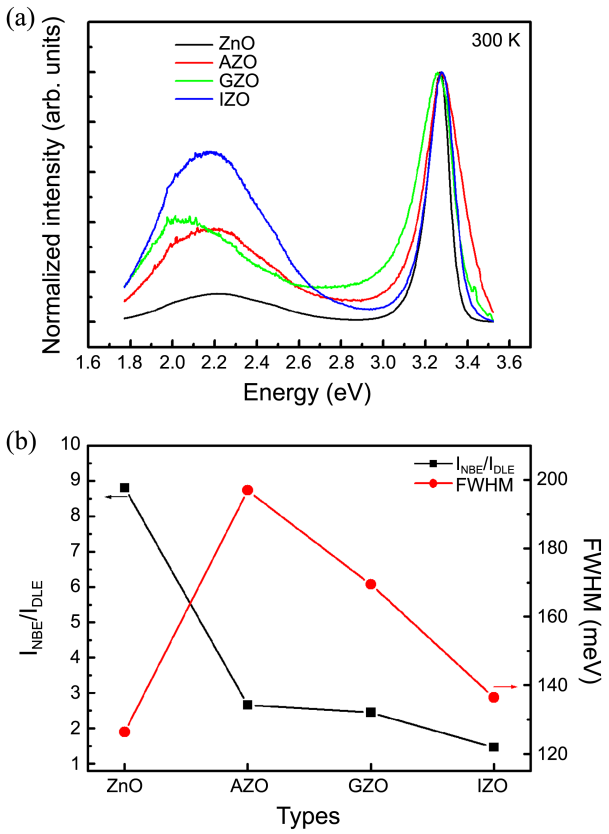

Figure 3. (a) Normalized PL spectra and (b) I_{NBE}/I_{DLE} and FWHM values of NBE exhibited by ZnO, AZO, GZO, and IZO nanorods.

ZnO nanorods. In addition, while ZnO, AZO, and IZO nanorods exhibited the green emissions, GZO nanorods showed orange emission (GZO). This phenomenon can be interpreted on the basis of interstitial and/or substitution reactions of dopants giving rise to the emission peaks with the differences in the radii between Zn and the dopant atoms and the lattice distortions causing the shift in the positions of the peaks. The lattice distortions may have resulted from defects such as oxygen states associated with lattice defects,[36,37] which are related to the DLE.

Figure 3(b) shows the ratios of the intensity of the NBE to that of the DLE (I_{NBE}/I_{DLE}) and the full width at half maximum (FWHM) of NBE for ZnO, AZO, GZO, and IZO nanorods. The I_{NBE}/I_{DLE} values shown by the ZnO, AZO, GZO, and IZO nanorods were 8.798, 2.659, 2.444, and 1.467, respectively. The ratios gradually decreased with increase in the atomic radius of the dopants. The FWHM of NBE values shown by the ZnO, AZO, GZO, and IZO nanorods were 126, 196, 169, and 136 meV, respectively. The FWHM values shown by AZO, GZO, and IZO nanorods was higher than that shown by the ZnO nanorods and the values decreased with increasing atomic radii of the dopants. Hence, the dopants affected the PL properties of the ZnO nanorods and it is possible to tune the DLE as the need arises such as chemical gas sensors, solar cells, and lighting emitting diodes, etc.

Figure 4(a) shows the optical transmittance spectra of the

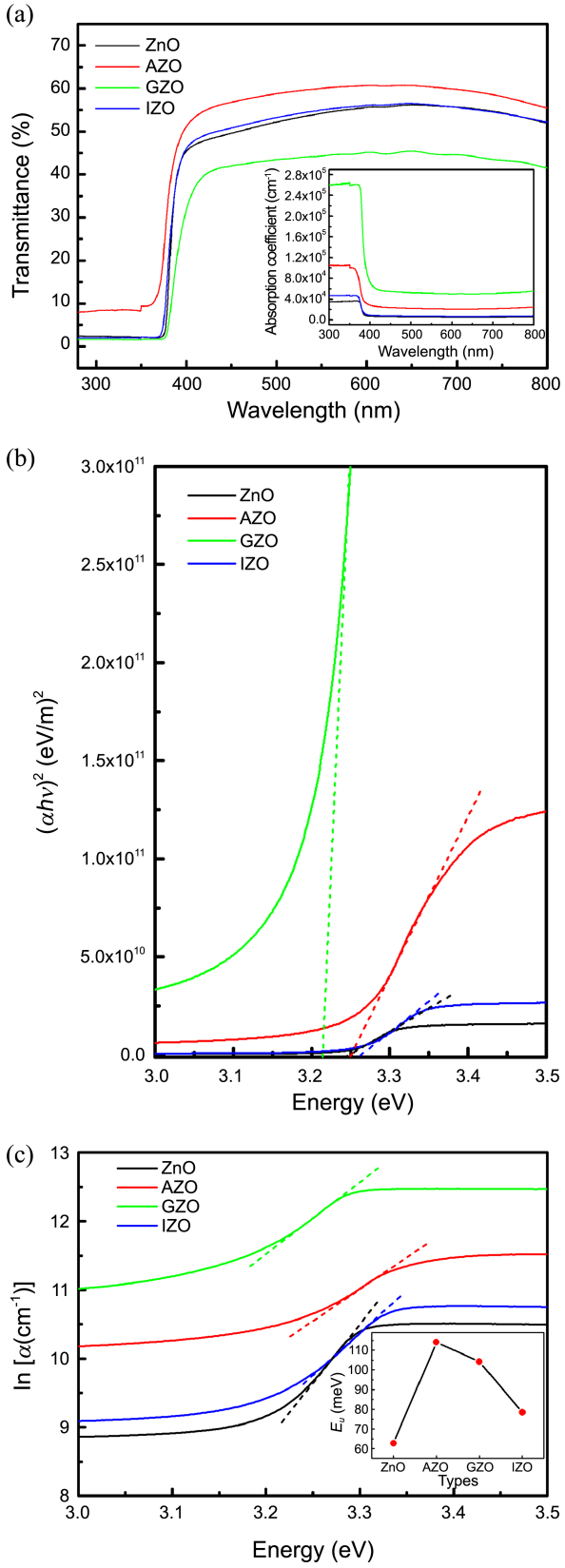

Figure 4. (a) Optical transmittance spectra (with the inset showing the variation of α with wavelength), (b) plots of $(\alpha h\nu)^2$ *vs.* photon energy, and (c) plots of lnα *vs.* photon energy (with the inset showing variation in E_U with various dopants) shown by ZnO, AZO, GZO, and IZO nanorods.

ZnO, AZO, GZO, and IZO nanorods. The inset shows the variation of absorption coefficients (α) with the wavelength, obtained from the equation $I = I_0 e^{-\alpha d}$, where I and I_0 are the intensities of the transmitted and incident light, respectively, and d is the thickness of the nanorods. In general, the optical transmittance is known to be affected by d, α, and surface roughness values. The absorption coefficient ($\alpha(\lambda)$) of the ZnO-based materials can be calculated from the optical transmittance (T) by the following equation:[38]

$$T = \exp[-\alpha(\lambda)d] \tag{15}$$

In comparison to the ZnO nanorods, the AZO nanorods exhibited significantly improved transmittance. The IZO nanorods showed more enhanced transmittance in the visible region. Interestingly, although the growth of GZO nanorods was low when compared with the other nanorods, their transmittance values were lower than that shown by ZnO nanorods. This may be due to the deposition of Ga dopants on the ZnO seed layers during nanorods growth by the hydrothermal method, leading to localized surface plasmon resonance.[39,40] Therefore, the amount of absorbance increased, as shown in the inset of Figure 4(a). The absorption edges from the AZO and IZO nanorods samples obtained in this study gradually blue-shifted due to the presence of the different dopants and that originating from the GZO nanorods was red-shifted. It is to be noted that differences in the nanorod lengths and distortions in the ZnO lattice as well as the differences in the Zn-O bond lengths can influence the shifts in the absorption edges. The optical band gap of the nanorods can be obtained by analyzing the absorption edges and by applying the Tauc model[41] represented by the following relationship:

$$\alpha h\nu = B(h\nu - E_g)^{1/2} \tag{16}$$

where h is the Planck's constant, ν is the frequency of the incident photons, and B is a constant that depends on the electron-hole mobility. Figure 4(b) shows the plots of $(\alpha h\nu)^2$ as a function of the photon energy for the ZnO, AZO, GZO, and IZO nanorods. The values of optical band gaps of ZnO, AZO, GZO, and IZO nanorods were found to be 3.245, 3.251, 3.218, and 3.262 eV, respectively, which implies that the optical band gap was affected by the various dopants. The optical band gaps of the AZO and IZO nanorods clearly shifted towards the blue region and the optical band gaps of the GZO nanorods shifted towards the red region, when compared with the band gap of the ZnO nanorods. Consequently, the optical band gaps changed proportionally with shift in the absorption edge.

Figure 4(c) shows the variation of ln α as a function of photon energy, and the inset shows the variation of Urbach energy (E_U), which represents the width of the exponential absorption edge, with various dopants. The absorption coefficient near the fundamental absorption edge was found to be exponentially dependent on the incident photon energy, and obeyed the empirical Urbach relationship, in which ln α varies as a function of $h\nu$. E_U can be calculated using the

following relationship:[42]

$$\alpha = \alpha_0 \exp(h\nu/E_U) \quad (17)$$

where α_0 is a constant. The E_U values were calculated from the Urbach plots using the following relationship:

$$E_U = [d(\ln\alpha)/d(h\nu)] \quad (18)$$

The values of E_U for the ZnO, AZO, GZO, and IZO nanorods were 62.7, 114, 104, and 78.4 meV, respectively. The various dopants affected the widths of the localized states outside the optical band gap (*i.e.*, above the upper regions of the conduction band and/or below the lower limits of the valence band) of the ZnO nanorods, resulting in a change in the optical band gap. Thus, the E_U changed with the optical band gap, which can be inferred from the inset in Figure 4(c). Furthermore, the decrease in the E_U indicates that the crystal quality of the ZnO nanorods improved and that the crystallinity of the IZO nanorods, which exhibited the minimum E_U, was the highest among the doped nanorods. Hence, it is evident that the various dopants affected the optical properties of the ZnO nanorods.

Conclusions

ZnO seed layers were deposited on quartz substrate using the sol-gel method, and ZnO, AZO, GZO, and IZO nanorods were grown on these ZnO seed layers by hydrothermal method. The effects of doping on the structural and optical properties of the ZnO nanorods were investigated. All the nanorods, irrespective of the presence or absence of doping and the type of dopant, were uniformly hexagonal in shape. We could control the dimensions of the nanorods by adding various dopants during the nanorods growth and specifically, the diameter of the nanorods decreased with increasing dopant atomic number. Among the various nanorods samples (ZnO nanorods and samples doped with various metals), while GZO nanorods predominantly showed poor properties, AZO nanorods showed better structural and optical properties. IZO nanorods, which were present in uniform and dense arrays, as characterized by SEM, showed the highest levels of crystallinity. Hence, from our studies, we conclude that the presence of various types of dopants can affect the structural and optical properties of ZnO nanorods.

Acknowledgments. This research was supported by Basic Science Research Program Through the National Research Foundation of Korea (NRF) funded by the Ministry of Education, Science and Technology (No. 2012R1A1B3001837).

References

1. Willander, M.; Nur, O.; Zhao, Q. X.; Yang, L. L.; Lorenz, M.; Cao, B. Q.; Pérez, J. Z.; Czekalla, C.; Zimmermann, G.; Grundmann, M.; Bakin, A.; Behrends, A.; Suleiman, M. A.; Shaer, A. E.; Mofor, A. C.; Postels, B.; Waag, A.; Boukos, N.; Trvalos, A.; Kwack, H. S.; Guinard, J.; Dang, D. L. S. *Nanotechnology* **2009**, *20*, 332001.
2. Guo, H.; Zhou, J.; Lin, Z. *Electrochem. Commun.* **2008**, *10*, 146.
3. Chu, S.; Olmedo, M.; Yang, Z.; Kong, J.; Liu, J. *Appl. Phys. Lett.* **2008**, *93*, 1811106.
4. Zhu, Y. W.; Zhang, H. Z.; Sun, X. C.; Feng, S. Q.; Xu, J.; Zhao, Q.; Xiang, B.; Wang, R. M.; Yu, D. P. *Appl. Phys. Lett.* **2003**, *83*, 144.
5. Fan, Z.; Lu, J. G. *Appl. Phys. Lett.* **2005**, *86*, 123510.
6. Kim, D.; Yun, I.; Kim, H. *Curr. Appl. Phys.* **2010**, *10*, S459.
7. Tubtimtae, A.; Lee, M.-W. *Superlattices. Microstruct.* **2012**, *52*, 987.
8. Yang, H.; Lee, J.-S.; Bae, S.; Hwang, J. H. *Curr. Appl. Phys.* **2009**, *9*, 797.
9. Fang, T.-H.; Kang, S.-H. *J. Phys. D: Appl. Phys.* **2008**, *41*, 245303.
10. Kim, S.; Kim, M. S.; Nam, G.; Lee, J.-Y. *Electron. Mater. Lett.* **2012**, *8*, 445.
11. He, H. P.; Tang, H. P.; Ye, Z. Z.; Zhu, L. P.; Zhao, B. H.; Wang, L.; Li, X. H. *Appl. Phys. Lett.* **2007**, *90*, 023104.
12. Zhu, L.; Li, J.; Ye, Z.; He, H.; Chen, X.; Zhao, B. *Opt. Mater.* **2008**, *31*, 237.
13. Nayak, P. K.; Yang, J.; Kim, J.; Chung, S.; Jeong, J.; Lee, C.; Hong, Y. *J. Phys. D: Appl. Phys.* **2009**, *42*, 035102.
14. Morales, A. E.; Zaldivar, M. H.; Pal, U. *Opt. Mater*, **2006**, *29*, 100.
15. Fang, T.-H.; Kang, S.-H. *Curr. Appl. Phys.* **2010**, *10*, 1076.
16. Chien, F. S.-S.; Wang, C.-R.; Chan, Y.-L.; Lin, H.-L. *Sens. Actuators B* **2010**, *144*, 120.
17. Oh, S.; Jung, M.; Koo, J.; Cho, Y.; Choi, S.; Yi, S.; Kil, G.; Chang, J. *Physica E* **2010**, *42*, 2285.
18. Cho, M. Y.; Kim, M. S.; Choi, H. Y.; Yim, K. G.; Leem, J.-Y. *Bull. Korean Chem. Soc.* **2011**, *32*, 880.
19. Kim, D. Y.; Kim, S.-O.; Kim, M. S.; Yim, K. G.; Kim, S.; Nam, G.; Lee, D.-Y.; Leem, J.-Y. *J. Korean Phys. Soc.* **2012**, *60*, 94.
20. Tian, Z.; Voigt, J. A.; Liu, J.; Mckenzie, B.; Mcdermott, M. J.; Rodriguez, M. A.; Konishi, H.; Xu, H. *Nat. Mater.* **2003**, *2*, 821.
21. Nunes, P.; Fortunato, E.; Tonello, P.; Fernandes, F. B.; Vilarinho, P.; Martins, R. *Vacuum* **2002**, *64*, 281.
22. Hong, C.-S.; Park, H.-H.; Moon, J.; Park, H.-H. *Thin Solid Films* **2006**, *515*, 957.
23. Sim, K. U.; Shin, S. W.; Moholkar, A. V.; Yun, J. H.; Moon, J. H.; Kim, J. H. *Curr. Appl. Phys*. **2010**, *10*, S463.
24. Ramalingam, R. J.; Chung, G. S. *Mater. Lett*. **2012**, *68*, 247.
25. Yim K. G.; Jeon, S. M.; Kim, M. S.; Kim, S.; Nam, G.; Lee, D.-Y.; Kim, J. S.; Kim, J. S.; Leem, J.-Y. *Acta Phys. Pol. A* **2012**, *121*, 214.
26. Kim, M. S.; Yim, K. G.; Choi, H. Y.; Cho, M. Y.; Kim, G. S.; Jeon, S. M.; Lee, D.-Y.; Kim, J. S.; Son, J.-S.; Lee, J. I.; Leem, J.-Y. *J. Cryst. Growth* **2011**, *326*, 195.
27. Kim, M. S.; Yim, K. G.; Kim, D. Y.; Kim S.; Nam, G.; Lee, D.-Y.; Kim, S.-O.; Kim, J. S.; Kim, J. S.; Son, J.-S.; Leem, J.-Y. *Electron. Mater. Lett.* **2012**, *8*, 75.
28. Kim, M. S.; Yim, K. G.; Cho, M. Y.; Kim, S.; Nam, G.; Lee, D.-Y.; Kim, J. S.; Kim, J. S.; Son, J.-S.; Lee, J. I.; Leem, J.-Y. *AIP Conf. Proc.* **2011**, *1400*, 443.
29. Baruah, S.; Dutta, J. *Sci. Technol. Adv. Mater.* **2009**, *10*, 013001.
30. Li, W.-J.; Shi, E.-W.; Zhong, W.-Z.; Yin, Z.-W. *J. Cryst. Growth* **2009**, *203*, 186.
31. Heller, R. B.; McGannon, J.; Weber, A. H. *J. Appl. Phys.* **1950**, *21*, 1283.
32. Nam, G.; Kim, S.; Kim, M. S.; Yim, K. G.; Kim, D. Y.; Kim, S.-O.; Leem, J.-Y. *J. Korean Phys. Soc.* **2011**, *59*, 129.
33. Jeon, J.-W.; Kim, M.; Jang, L.-W.; Hoffman, J. L.; Kim, N. S.; Lee, I.-H. *Electron. Mater. Lett.* **2012**, *8*, 27.
34. Kim, M. S.; Yim, K. G.; Kim, S.; Nam, G.; Lee, D.-Y.; Kim, J. S.; Kim, J. S.; Leem, J.-Y. *J. Korean Phys. Soc.* **2011**, *59*, 2354.
35. Kim, M. S.; Yim, K. G.; Lee, D.-Y.; Kim, J. S.; Kim, J. S.; Leem, J.-Y. *J. Korean Phys. Soc.* **2011**, *58*, 821.
36. Liao, Z.-M.; Zhang, H.-Z.; Zhou, Y.-B.; Xu, J. Zhang, J.-M.; Yu, D.-P. *Phys. Lett. A* **2008**, *372*, 4505.
37. Djurišic, A. B.; Leung, Y. H.; Tam, K. H.; Ding, L.; Ge, W. K.; Chen, H. Y.; Gwo, S. *Appl. Phys. Lett.* **2006**, *88*, 103107.

38. Kim, M. S.; Yim, K. G.; Kim, S.; Nam, G.; Lee, D.-Y.; Kim, J. S.; Kim, J. S.; Leem, J.-Y. *Acta Phys. Pol. A* **2012**, *121*, 217.
39. Mulvaney, P. *Langmuir* **1996**, *12*, 788.
40. Barnes, W. L.; Dereux, A.; Ebbesen, T. W. *Nature*, **2003**, *424*, 824.
41. Jain, A.; Sagar, P.; Mehra, R. M. *Solid-State Electron.* **2006**, *50*, 1420.
42. Kim, M. S.; Kim, T. H.; Kim, D. Y.; Kim, S.-O.; Lee, D.-Y.; Kim, J. S.; Kim, J. S.; Son, J.-S.; Leem, J.-Y. *J. Korean Phys. Soc.* **2012**, *60*, 830.